Coastal Engineering 60 (2012) 123–135

Contents lists available at SciVerse ScienceDirect

Coastal Engineering

journal homepage: www.elsevier.com/locate/coastaleng

Laboratory investigation of dune erosion using stereo video

Margaret L. Palmsten [a,b,*], Robert A. Holman [a]

[a] College of Oceanic and Atmospheric Science, Oregon State University, 104 COAS Administration Building, Oregon State University, Corvallis, OR, 97331, USA
[b] Code 7430, Naval Research Laboratory, Stennis Space Center, MS, 39529, USA

ARTICLE INFO

Article history:
Received 11 August 2010
Received in revised form 7 September 2011
Accepted 8 September 2011
Available online 7 October 2011

Keywords:
Stereo imaging
Dune erosion
Wave runup
Remote sensing

ABSTRACT

Simple parameterizations of dune erosion are necessary for forecasting erosion potential prior to an oncoming storm. Dune erosion may be parameterized in terms of the elevation of the total water level (composed of surge, tide, and wave runup) above the dune base and period of exposure of the dune to waves. In this work, we test several versions of this model using observations from a large wave tank experiment designed to model a storm hydrograph, and we develop a new method for acquiring the appropriate data with confidence intervals using stereo video techniques.

The stereo method results in observations of dune morphology at higher spatial and temporal resolutions than traditional survey methods allow. Resolution of the stereo technique was 0.1 m in the horizontal and 0.04 m in the vertical, and errors in stereo observations were on the order of 0.02 to 0.08 m (1 to 2 pixels) when compared with surveys. A new method was developed to estimate confidence intervals on stereo observations. When the unchanging dune top was repeatedly sampled, the new confidence intervals encompassed 2 standard deviations of scatter about the mean dune surface 98% of the time.

Observations from the stereo method were used to quantify wave runup and dune erosion. We tested a variety of runup statistics based on a Gaussian distribution of swash properties, and found that the most predictive statistic for dune erosion was the 16% exceedance elevation above the dune base, lower than the often used 2% exceedance value. We found that the parameterization of runup was sensitive to the definition of beach slope and that the most accurate beach slope for predicting runup was through the region of the beach profile defined by the mean water level plus one standard deviation of swash. The dune base retreated along a relatively constant trajectory that was a half of the initial beach slope. Finally, a simple model for dune erosion was tested and found to reproduce 64% of the observed variance in dune erosion rate given known forcing at the dune and 49% of the observed variance in dune erosion rate given parameterized forcing. Integrating the simple model over time, 93% of the observed dune retreat distance was reproduced given offshore forcing.

1. Introduction

Coastal sand dunes are known as the "first line of defense" against the combination of high water levels and large waves generated by extreme storms. When water levels overtop the dune crest, sensitive habitat and structures are at risk. In recent years, associated damages have reached billions of dollars (Changnon, 2000). In order to plan for and mitigate damage caused by extreme storms, a firm physical understanding of the interplay between fluid and sediment transport causing dune erosion must be developed. The matter is even more pressing in the face of higher waves (Allan and Komar, 2006), increased water levels (IPCC, 2007), and changing storm tracks (Graham and Diaz, 2001) caused by climate change.

This paper has two objectives. Our primary goal is to test models and a number of concepts related to dune erosion using data from a wave tank experiment in which forcing conditions mimicked a well-documented natural storm. Our second goal is to develop and test a stereo-based approach that allows collection of high-resolution data with confidence intervals without the interference normally associated with in situ sampling.

Two types of dune erosion models will be tested. The simplest models include only one parameter, the relationship between water level and specific dune features, without including information about time dependent forcing or feedback with morphology. This is best illustrated by the Storm Impact Scaling (Sallenger, 2000) which defines a set of erosion risk conditions based simply on whether the height of the total water level exceeds the elevation of the dune base, z_b, (collision regime) or dune crest, z_c (overtopping regime). While erosion rate is not specified, it is assumed that the magnitude of erosion is strongly dependent on regime so that regime identification will be an adequate indicator of net erosion.

The total water level includes contributions from tide and surge that can be found from regional models, but also from wave runup. Sallenger (2000) suggested the use of the 2% exceedance value of

* Corresponding author at: Code 7430, Naval Research Laboratory, Stennis Space Center, MS, 39529, USA. Tel.: +1 228 688 5475; fax: +1 228 688 5752.
E-mail address: margaret.palmsten.ctr@nrlssc.navy.mil (M.L. Palmsten).

0378-3839/$ – see front matter © 2011 Elsevier B.V. All rights reserved.
doi:10.1016/j.coastaleng.2011.09.003

runup, R_2, as appropriate to dune impact assessment, although alternative exceedance values were not tested. Determining the most appropriate exceedance value will be one focus of this study.

Based on an extensive data set of video observations from ten experiments from a variety of beaches, Stockdon et al. (2006) provided an equation relating R_2 to bulk environmental conditions assuming a slightly non-Gaussian relation between runup and swash

$$R_2 = 1.1\left(0.35\beta(H_0L_0)^{1/2} + \frac{\left[H_0L_0\left(0.563\beta^2 + 0.0004\right)\right]^{1/2}}{2}\right). \quad (1)$$

H_0 is the offshore significant wave height, L_0 is the offshore wavelength and β is the foreshore beach slope. The first term in Eq. (1) represents the contribution of mean water level, $\langle\eta\rangle$, to runup, and the second term represents the contribution due to two standard deviations of swash, $2\sigma_s$. In the original paper, Stockdon et al. used the mean slope in the region of active swash (defined as the region between $\langle\eta\rangle \pm 2\sigma_s$) as the value for the foreshore beach slope, $\beta_{2\sigma}$. However, storm waves are likely to rapidly flatten the foreshore profile rendering pre-storm measurements of $\beta_{2\sigma}$ irrelevant for predicting subsequent dune erosion. To compensate for the change in location of the swash zone during storms, Stockdon et al. (2007) approximate a storm value of $\beta_{2\sigma}$, β_s, as the mean slope between the still water line and the base of the dune. The definition of β_s is further complicated under dune erosion conditions, when swash is acting over both a foreshore and scarp slope, which may vary rapidly as the dune slumps. Feedback between storm runup, the foreshore slope and the resulting dune erosion will also be a focus of this study.

While the Storm Impact Scaling provides a useful classification of the potential for dune erosion, it does not quantify the magnitude of erosion, or account for time-varying wave forcing. A second approach that does model time dependent erosion is the wave impact model (Fisher et al., 1986; Overton and Fisher, 1988; Overton et al., 1994). This model hypothesizes that the volume erosion rate of the dune is linearly proportional to the momentum flux impacting the dune face, or

$$\Delta V = C_c \sum F \quad (2)$$

where ΔV is the volume of eroded sediment, C_c is a calibration coefficient, and F is the force of impact per wave. The wave impact model was extended by Larson et al. (2004) (hereafter LEH04) to include an explicit dependence on both the runup elevation, R, and the duration of exposure, t

$$\Delta V = 4C_s(R - z_b)^2 \frac{t}{T} \quad (3)$$

where C_s is an empirical coefficient, T is the wave period and z_b is the elevation of the dune base. In LEH04, the appropriate value of runup, R, is assumed to be

$$R_L = 0.158\sqrt{H_{0rms}L_0} \quad (4)$$

where H_{0rms} is deep water root mean square wave height. Unlike Eq. (1), LEH04 neglected β and calibrated R_L for laboratory experiments where the mean value of β was 0.16. However, Eq. (1) assuming a constant β of 0.16 produces results nearly identical to Eq. (4) so the Larson equation effectively provides R_2 statistics. The coefficient, C_s, which parameterizes the physics of the interaction between hydrodynamics and sediment, depends on the ratio between H_{0rms} and median grain diameter.

The LEH04 formulation is attractive because it is derived from a physics-based impact model but is expressed in simple, intuitive terms. Is seems sensible that dune erosion should be related to the magnitude of exposure of the dune face, $(R - z_b)$, and also to the duration of that exposure, t/T, which can be thought of as the number of collisions between the runup and the dune. Ruggiero et al. (2001) and Pye and Blott (2008) also found the best predictor of magnitude of dune erosion on the Oregon and United Kingdom coasts was length of exposure to waves. In this paper we will test the LEH04 equation both in terms of the individual dependencies and the overall performance of the equation.

Dune erosion research has been slowed by the limited availability of good data. Typically, only pre- and post-storm observations of dune erosion are available from the field, because harsh conditions preclude making observations during storms. As a result, most of the observations used to develop and validate dune erosion models have come from near-prototype wave flume experiments. Large-scale experiments have the advantage of controlling hydrodynamic and sediment characteristics, and reducing the dune erosion problem to two dimensions. Dette et al. (2002) provides an extensive review of large scale experiments. More recently, van Gent et al. (2008) and van Thiel de Vries et al. (2008) describe a 2006 large scale dune erosion experiment in the Delta Flume, De Voorst, the Netherlands.

In this paper, we develop and test an optical remote sensing method to observe dune morphology on slump event timescales and estimate the net cross-shore transport across the dune and foreshore on timescales faster than surveys typically conducted in wave flumes and without interruption of wave forcing.

Previous large scale experiments have tested constant wave conditions until an equilibrium profile develops. However, this approach precludes understanding the sequencing of forcing. In this paper, we quantify time dependent dune erosion and wave runup by modeling a storm hydrograph during a dune erosion experiment. Later, we will show that the length of exposure to waves is nearly as important as knowing the details of water level for modeling dune erosion.

In Section 2, we introduce the theory of stereo sampling and adapt the principals of Holland and Holman (1997) to develop a binocular method for observing foreshore morphology based on time varying runup signals. Section 3 of this paper describes a near-prototype dune erosion experiment conducted at the O.H. Hinsdale Wave Research Lab. Section 4 describes the accuracy of the stereo remote sensing technique and quantifies changes of beach morphology. The final sections discuss implications of results for dune erosion models and describe conclusions.

2. Stereo methods

2.1. Stereo technique

The stereo method is composed of two main components, an automated feature matching algorithm required to determine the pixel disparity (D) between the same feature in either camera, and a triangulation algorithm to determine the stereo solution based on camera information and pixel disparity. The triangulation algorithm was formulated using the concept of homogeneous coordinates, a well-known mathematical formalism developed specially for computer vision that is described in detail by Hartley and Zisserman (2004) and not discussed further here. The success of the triangulation algorithm depends largely on the stereo resolution and error in feature matching that are described in Section 2.2. Two different feature matching algorithms were implemented, one for the subaerial beach, where many features are available for matching, and one algorithm for the swash zone, which is complicated by optical reflections. Finally, we developed a new equation for estimating confidence intervals on the stereo solution.

2.2. Theoretical stereo resolution and error

Error in determining the pixel location of a matching feature in a camera (ΔD) will result in an error in the elevation of the stereo measurement (Δz),

$$\Delta z = \frac{dz}{dD}\Delta D \quad (5)$$

where dz/dD is the stereo resolution of the camera. Since stereo resolution is a function of the camera orientation and internal camera parameters, dz/dD was estimated numerically. First, the pixel locations of (x, y, z) points within the camera view were determined. Then, a one-pixel shift ($dD = 1$ pixel) was introduced into the pixel locations and the stereo equation was solved to find the location of the shifted points $(x + dx,\ y + dy,\ z + dz)$. Finally, the shifted points are subtracted from the original points in the camera view to determine the theoretical resolution.

This equation has two applications. First, the vertical resolution of a single pixel for a particular stereo camera configuration can be determined by assuming a one-pixel shift in ΔD. Second, if ΔD is independently quantified as it is in Section 4.1, Eq. (5) gives the corresponding vertical error on the stereo estimate.

2.3. Feature matching techniques

Accurate feature matching is the key component to producing precise stereo results (Eq. (5)). Because there are abundant contrast features on the dune including variations in sediment color due to mineralogy, variations in water content, presence of organic material, residual foam, and morphologic features like the dune crest and base, correlation based feature mapping methods can be used. However the foreshore environment is complicated by specular reflections off saturated sediment, so requires an alternate methodology. In this section, we describe the algorithms, including improvements, used for each domain.

Stereo analysis of the dune face and top was based on a cross-correlation and dynamic programming algorithm originally developed by (Sun, 2002b). The algorithm is composed of several steps but is primarily based on finding the disparity, D (pixel distance between feature matches), that maximizes optical similarity, E (called evidence), for each pixel over the entire domain that is defined by u columns and v rows. Because evidence is based on a two dimensional convolution of fixed size, the images are first high-pass filtered to remove variance at larger scales. The map of evidence over the domain is then found for a range of plausible disparities. Finally, an optimum path is found through the evidence space so that unique values of disparity (Sun, 2002a), hence world location, can be found for every imaged location using triangulation.

A number of measures of feature similarity (evidence) have been proposed in the literature. We have based our analysis on the simple measure of lagged cross-correlation. The optimum correlation window size was determined by conducting a sensitivity test to minimize scatter in range direction on the beach surface. Correlation window sizes between 3 by 7 (rows by columns) and 41 by 41 were tested. The window size was set to 35 by 25 pixels, approximately 0.75 m × 0.25 m on the foreshore and dune, as the highest resolution window still with minimum scatter.

Stereo analysis on the foreshore is complicated by the frequent presence of a thin layer of water that generates specular reflectance, acting like a mirror. Stereo analysis of features seen in a planar mirror will yield the position of the virtual object location behind the mirror (beneath the beach) and will be significantly in error. In contrast, the strong scattering of light by the foam edge of wave runup is Lambertian, therefore seen identically in each camera, so is appropriate for stereo analysis. Since the runup edge lies along the foreshore by definition, time-varying runup position can be exploited to map the foreshore following the method of Holland and Holman (1997). Given the sensitivity of the stereo method, Eq. (5), the accuracy criteria for runup measurement for stereo use are more stringent than those for simple runup time series analysis and a two-step analysis was used. First the approximate runup location was found using a semi-automated technique to digitize the time stack, then the locations were fine-tuned using a one dimensional matching algorithm equivalent to that used on the dune.

Runup data were extracted from time stacks (Holman and Stanley, 2007), created from cross-shore pixel arrays located approximately along an epipolar line. An epipolar line is the projection of the line joining one camera center and a point in the image into the image from the second camera in the stereo pair (Hartley and Zisserman, 2004). However, deviations from the epipolar line of up to +/−2 pixels in the alongshore or approximately +/−2 cm in the foreshore region were considered insignificant since the runup edge is not expected to vary significantly over 2 cm in the alongshore direction.

The foam edge of a wave approaching the shoreline is visible as a bright streak through the time stack (Fig. 1). A semi-automated runup algorithm defines pixel location of the runup edge (v_r) as the landward-most location where the difference intensity, δI, between the image intensity, $I(v,t)$, and a background running average intensity, $I_{back}(v,t,)$ exceeds a user-specified threshold. This location is reliable for time series analysis of runup but is often several pixels landward of the base of the steep image intensity gradient marking the runup front. A better estimate of position of the advancing runup front, v_{rf}, is given by the location of maximum curvature in the intensity profile, $\partial^2 I/\partial v^2$ in a search region defined by the inflection points in $\partial I/\partial v$ onshore and offshore of the digitized runup edge. Of the signals from the two cameras, the one with the greater curvature is taken as the reference runup, v_{rf}.

To find the matching location, a lagged correlation is used to shift the runup position in the camera with lower signal strength (curvature) to match v_{rf}. Following the work of Sun (2002b), the correlation coefficient is recast as E. Minimum E defines the corrected pixel location of runup in the camera with the weaker signal. Once the pixel coordinates giving the best match between runup features in both cameras are obtained $(v_{rf1},\ v_{rf1} + D)$, the 3D position of the feature is determined using triangulation.

The resolution of a surface derived from the above stereo techniques is limited by the discrete pixel resolution. However, fitting methods following Sun (2002b) were used to achieve subpixel resolution, thereby improving accuracy.

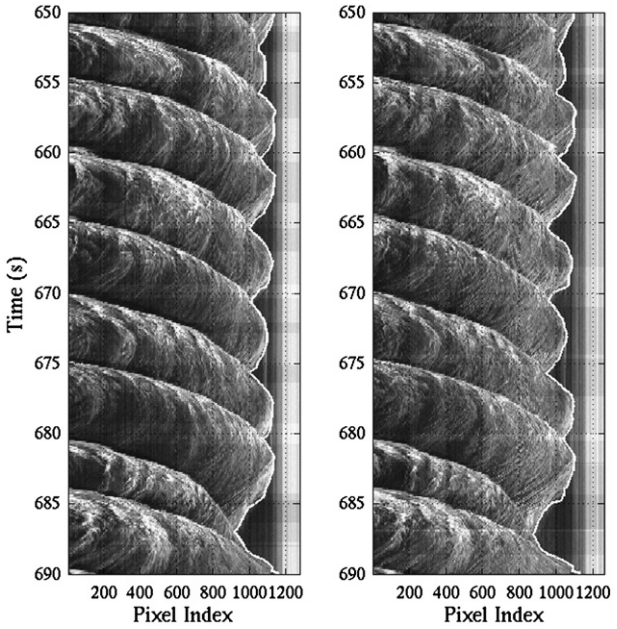

Fig. 1. Time stacks of the cross-shore transect of pixels for C_1 (left) and C_2 (right). The bores are visible in the time stacks as the bright streaks moving from left to right across the images. The digitized swash edge is denoted by the solid white line. The pixel location of the swash edge was projected onto the beach profile to determine the elevation of the swash edge.

2.4. Error thresholds

Error in stereo estimation may be grouped into three categories: 1) error due to camera hardware, including lens distortion and sensor noise; 2) error due to the stereo algorithm, including resampling, correlation window size, matching algorithm, 3) error due to the scene, including image geometry, lighting, and low image variance (Egnal et al., 2004). The first category is dependent on intrinsic camera properties, and not directly on the stereo algorithm or image contrast. In this section, we define three objective thresholds obtained from the feature matching process to quantify and minimize errors described in the last two categories. First, we removed all feature matches where correlation between features was negative ($\rho<0$). Second, we removed all feature matches where the high-passed image variance was too low to produce good feature matches ($\sigma^2<0.01$). Finally, we removed all matches where curvature of the $E(v,D)$ surface was low ($\alpha_1<0.01$), indicating a poorly defined feature match caused by low image variance, low resolution, or poor lighting. Later, in the Experimental results section, we define a relationship between α_1 and scatter to define error in terms of D that is related to error in real world coordinates via Eq. (5).

2.5. Interpolation

Results from the stereo method were spatially smoothed in space and time to reduce noise. Since errors in stereo estimates were defined in range direction (r) from the landward most camera, C_1, data were interpolated in (u,v,r) space, then transformed to (x,y,z) via the look direction from the center of C_1 to each pixel. An advantage of interpolating in range direction is resolution of the steep or potentially overhanging dune scarp, which would be obscured if the dunes were interpolated in the cross-shore direction. Interpolation was carried out in both space and time using a linear smoother with a Hanning filter (Plant et al., 2002) in space and boxcar averaging in time. For the dune region, the length scales of spatial smoothing window were set to the same length as the correlation window (35 pixels, 25 pixels) in (u,v) to achieve a final horizontal cross-shore resolution of approximately 0.1 m. Estimates were also time-averaged over 5 images, collected over 120 s (sub-samples taken every 30 s) between periods when waves were run, to reduce noise. For the foreshore, the length scale of smoothing was 25 pixels in v. Stereo estimates collected during the 15 minute wave run were averaged to fully map the beach profile and reduce noise.

2.6. Runup elevation measurements

The vertical elevation of runup was determined by projecting the beach profiles generated by the stereo method back into image coordinates. From the vertical elevation data associated with each pixel location, runup time series pixel data were converted to vertical elevation by linear interpolation.

3. Experiment description

3.1. O.H. Hinsdale large wave flume

The dune experiment was conducted at the Oregon State University O.H. Hinsdale Wave Research Lab in the Large Wave Flume. The flume is 107 m in length, 3.7 m in width, and 4.6 m in depth at the wave maker. The hinged wave maker was capable of producing monochromatic and random waves with a maximum wave height of 1.6 m with a period of 3.5 s. The origin of the wave flume coordinate system is located at the center of the base of the wave maker. A beach was created at the far end of the wave flume using 611 m^3 of Oregon beach sand with median grain size of 0.23 mm. The initial beach profile (Fig. 2) consisted of a flat bottom for 35 m shoreward of the wave maker, a relatively planar sand beach intersecting with the still water level near $x=80$ m, a steep foreshore ($\beta_s=0.17$) and dune.

3.2. Wave conditions

The experimental wave conditions were designed to be representative of the Northeaster' storm conditions that occurred offshore of Assateague Island, MA/VA, USA on February 3–8, 1998. This storm was chosen as the prototype for our experiment because offshore wave conditions were recorded and pre- and post-storm beach topographies were collected with lidar. The dunes retreated between 0 m and 30 m, depending upon alongshore location (Fauver, 2005). Prototype wave conditions at NOAA Buoy 44004, located at (38.48 N, 70.43 W), 370 km east of Cape May, NJ, indicated a maximum significant wave height of 7.35 m; maximum peak period of 12.5 s; and maximum storm surge of 1.03 m. Conditions modeled in the laboratory were determined by Froude scaling (Dean and Dalrymple, 2002) with a model length scale 1/6 of prototype and resulting time factor of $1/\sqrt{6}$. In Fig. 3, the thick lines represent wave conditions modeled in the lab. Maximum significant wave height modeled in the flume was 1.3 m; maximum peak wave period was 4.90 s; and maximum storm

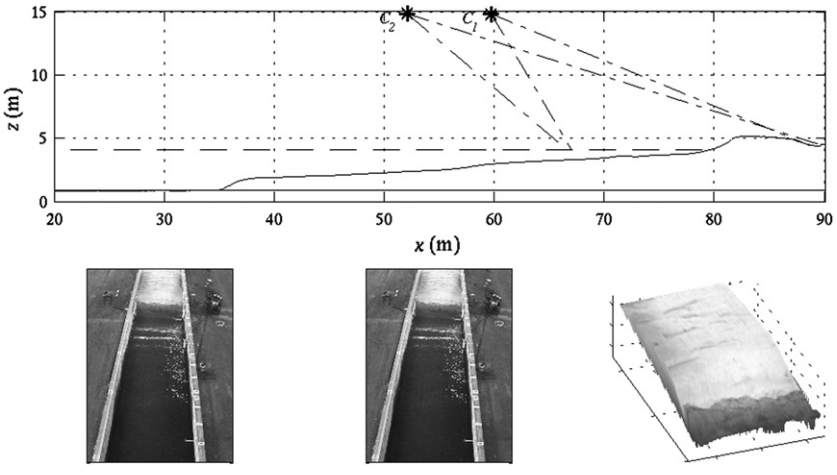

Fig. 2. The elevation view of the beach profile and camera positions (upper panel) is plotted in the wave flume coordinate system. The views from C_1 (lower left) and C_2 (lower middle) are used to create a stereo image of the dune and foreshore. Finally, the stereo view of the dry beach is draped with the image (lower right).

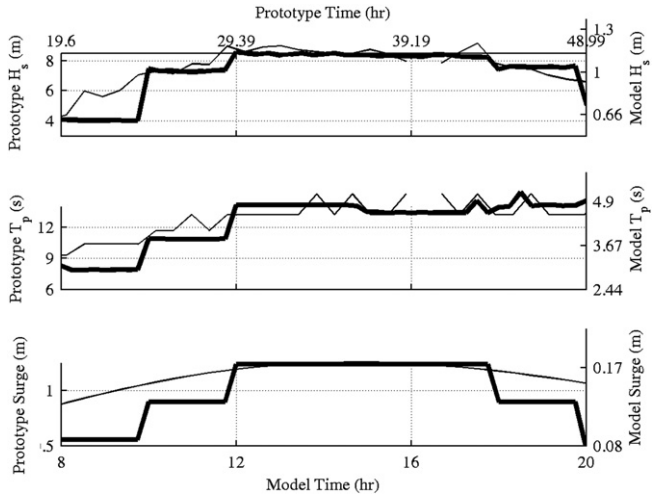

Fig. 3. The prototype (thin line) and modeled wave conditions (thick lines) at the wave maker throughout the dune erosion experiment were based on observations of the Northeaster storm that hit Assateauge Island, MD/VA, USA in February 1998 to reproduce the effect of temporally variable wave conditions acting on a dune. The spatial scaling between prototype and model is 1/6 and the temporal scaling is $1/\sqrt{6}$.

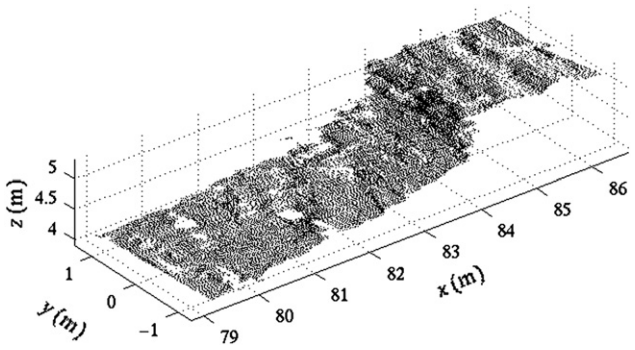

Fig. 4. The 3-dimensional beach surface is plotted. Each point represents a single raw stereo estimate from a pixel on the dune to demonstrate the density of data produced by the stereo technique. Only half of the raw points are plotted to allow better visibility of the dune.

surge was 0.17 m. The duration of maximum storm conditions during the experiment was 6 h. The wave maker was programmed with a TMA spectrum of appropriate significant wave height and peak period and random phase. The experiment was carried out in 15 minute increments; then the standing wave energy was allowed to settle before the test continued. Results from hours 8–20 of the experiment, when dune erosion occurred, will be discussed in this paper. Prior to hour 8 of the experiment, low wave conditions, representing pre-storm conditions, resulted in minimal sediment transport and no dune erosion. Dune erosion occurred when waves exceeded the dune base, and the primary mechanism of erosion was slumping of sediment from the dune that was then carried offshore via swash zone processes.

3.3. Profile surveys

In situ beach profiles were collected using two methods depending upon the region of the beach being measured. The subaqueous profile was determined using an acoustic sensor, while the subaerial profile was collected using a laser range finder. The profiling equipment in the flume was mounted on a motorized cart at $y = -0.86$ m in the alongshore. The cart was driven along the length of the flume to collect a profile. Profiles were collected every hour throughout the experiment. Vertical and horizontal resolutions of the profiling system were estimated to be 0.02 m. A cement step at the back of the wave flume was surveyed 31 times with the laser range finder over the course of the experiment. The standard deviation of elevation observations was 0.007 m.

3.4. Cameras

A stereo pair of Point Gray Scorpion charged couple device cameras was mounted on the roof of the Oregon State University O.H. Hinsdale Large Wave Flume looking downward into the flume from an elevation of 15 m (Fig. 2) above the flume floor (about 9 m above the still water line). Image resolution was 960×1280 pixels. The cameras were calibrated and surveyed to determine image geometry. Cross-shore resolution of the cameras was approximately 3 cm and alongshore resolution was approximately 1 cm near the foreshore and dune. Theoretical stereo resolution, determined using Eq. (5), was approximately 0.10 m by 0.01 m in the horizontal directions for the foreshore and dune but ranged between 0.005 m and 0.18 m over the field of view. Vertical stereo resolution was 0.04 m for the foreshore and dune region of interest but ranged between 0.015 m and 0.05 m over the field of view. Cross-shore transects of pixel intensity were collected from both cameras at 10 Hz at $y = 0$ m, down the center of the wave flume for runup measurement (Fig. 1) Synchronous full images were collected by each camera at 2.5 Hz for stereo analysis.

4. Stereo results

4.1. Spatial coverage, scatter, and bias

The most significant advantage of the stereo method is the high spatial resolution on the beach surface (Fig. 4), combined with estimates of

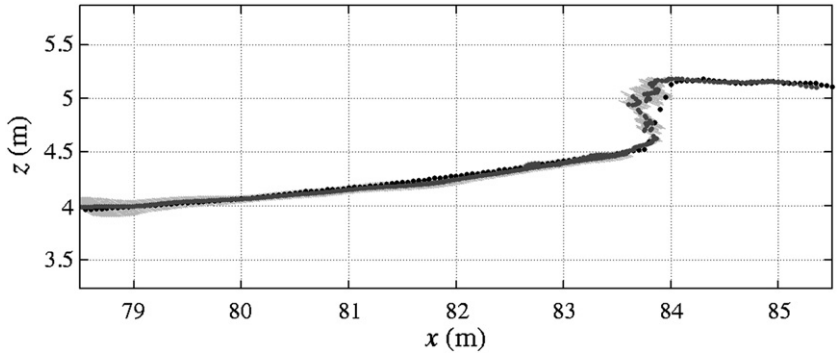

Fig. 5. The smoothed stereo observations (dark gray dots) combining data from the area-based stereo method applied on the dune and the runup-based stereo method on the foreshore are plotted at 13 h into the experiment. Error bars from Eqs. (5) and (6) are plotted in light gray lines, and the surveyed profile is plotted in black dots. RMSE was largest for the whole experiment at this time because of the smoothing of dune scarp by the correlation window that resulted in the overhang at the dune scarp.

error from the stereo method (Fig. 5) and bias, all at higher temporal resolutions than traditional surveys allow. Point density of raw stereo estimates was 1589 points/m^2 over the dune top, 2698 points/m^2 over the dune scarp, and 3756 points/m^2 over the foreshore. Scatter of raw stereo estimates was normally distributed (significant at the 95% level) in range direction about the mean dune surface.

To estimate confidence intervals on stereo estimates, 200 realizations of the unchanging top of the dune (away from the dune crest) were collected and the standard deviation in disparity, σ_D, was found at each pixel location from the ensemble. These values were regressed against a number of quality variables. In the end, the linear relationship

$$2\sigma_D = -26.66\alpha_1 + 2.55 \tag{6}$$

where α_1 is curvature of $E(D)$, was found to explain 90% of the data and provides a useful method of estimating confidence intervals exclusively from image data.

To further test the efficacy of the confidence interval calculated according to Eq. (6) at parameterizing scatter in the data, the error bars for this ensemble of unchanging locations were normalized as

$$\sigma_n = \frac{2|r-\mu_r|}{\sigma_r} \tag{7}$$

where σ_r is the confidence interval described in Eq. (6) projected to range from C_1, r is the range for each individual estimate, and μ_r is the mean location of the dune surface in range direction. Assuming scatter is normally distributed, and confidence intervals are uniformly distributed, the standard deviation of the normalized error bars should be 1 for error bars that perfectly parameterize scatter. 98% of σ_n ranged between 0 and 2 over the region of interest and 62% of σ_n ranged between 0 and 1 (Fig. 6) indicating that σ_r is representative of scatter about the mean.

4.2. Stereo-survey comparison

To test the quality of stereo results, bias and root mean square error (RMSE) in elevation were calculated for the stereo observations coincident with the 16 surveyed dune profiles during the experiment (Fig. 7), along with errors over the foreshore, scarp, and dune top. Over the full profile, average bias was −0.01 m, but ranged between

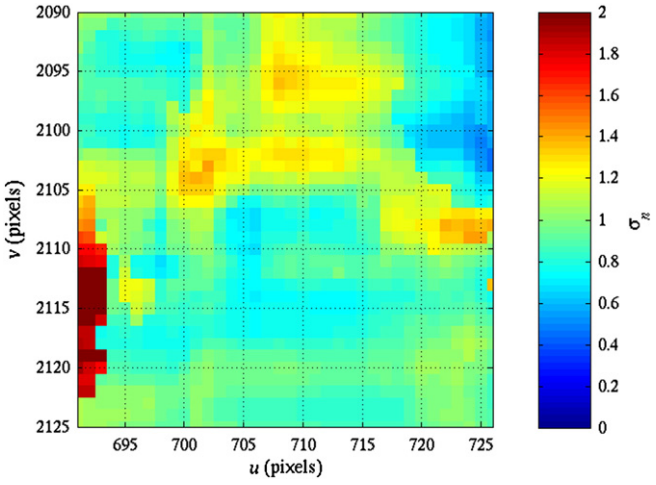

Fig. 6. The scatter in stereo results scaled by error bars is plotted over a stationary section of dune onshore of the crest. This plot demonstrates that the error bars are representative of scatter in stereo observations because the standard deviation of scatter scaled by error bars should be 1 if error bars perfectly quantify scatter. 98% of the data in this plot fall between 0 and 2 standard deviations of scatter and 62% of the data fall between 0 and 1.

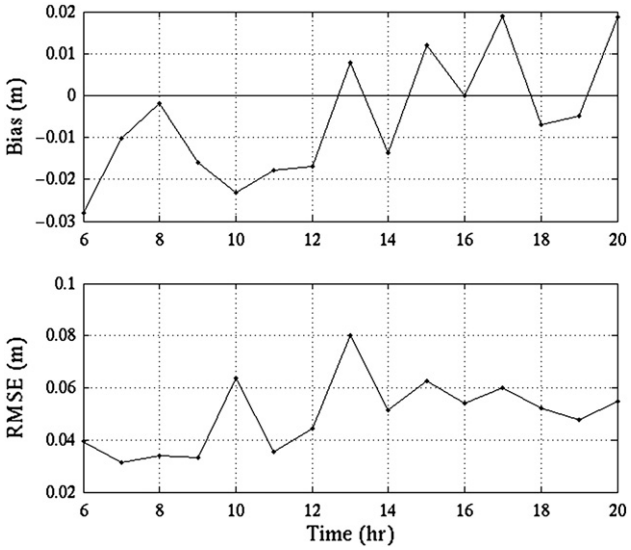

Fig. 7. The bias between the stereo and the surveyed beach profile was between −0.03 m and 0.02 m over the course of the experiment. RMSE between the stereo and surveyed profiles was 0.03 m and 0.08 m over the experiment, approximately the resolution of 1 to 2 pixels.

−0.03 m and 0.02 m throughout the experiment, and the average RMSE was 0.05 m, but ranged between 0.03 m and 0.08 m. These errors are equivalent to errors of 1 to 2 pixels, based on stereo resolution (Eq. (5)). Of the three subsections of the dune, bias and RMSE were largest over the dune scarp where the stereo method typically produced an overhanging dune, while an overhang was not observed qualitatively or in surveys. The mean horizontal error caused by the overhang was 0.09 m and RMSE was 0.13 m, equivalent to errors of approximately 1 pixel. The overhang was created by the smoothing effect of the correlation window in disparity space as the correlation window passed over the dominant optical feature associated with the dune scarp. When the smoothed surface was translated from disparity space to real world coordinates via triangulation, the overhang was produced (Fig. 5) and the resulting dune scarps have dune crests shifted offshore of the true position. The overhang effect is most pronounced on images with low contrast on the dune front and when the dune is farthest from the camera, resulting in low pixel resolution. At best, the confidence intervals correctly estimate error due to the overhang. At worst, the confidence intervals underestimate the overhang by 0.18 m (Fig. 5).

5. Experimental results

Our analysis will be framed around Eq. (3), which relates eroded volume of the dune to the fluid forcing in terms of the magnitude and duration of runup exceedance above the dune base. First, we examine each forcing element in terms of observations and expectations from parameterizations. Next, we compare each element with observed dune erosion. Finally, we couple the observed and parameterized forcing elements using the Eq. (3) and compare results with observed dune erosion.

5.1. Beach profiles and dune erosion

Beach profiles were extracted from stereo data down the tank center every 15 min while the dune was slumping. The 15 minute temporal resolution was controlled by two factors. First, dune slumping was episodic and occurred at a rate of approximately 1 slump per 15 min. Second, the runup stereo technique required approximately 15 min of data to fully map the foreshore. Fig. 8 shows the retreat of the dune over the course of the experiment. The dune crest (x_c, z_c)

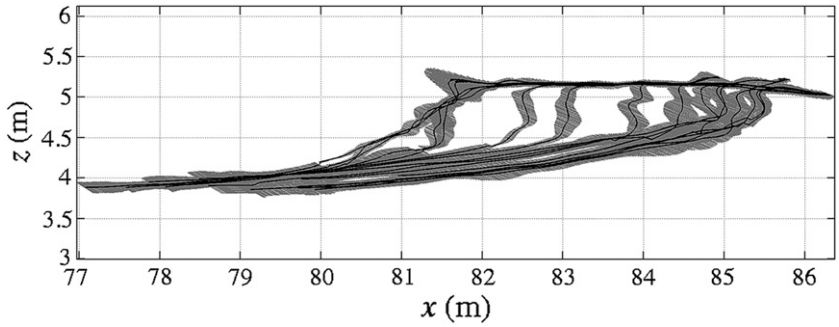

Fig. 8. Every 4th beach profile from stereo is plotted throughout the experiment with error bars in gray. The dune base rapidly retreated leaving a steep scarp that migrated landward throughout the experiment.

and dune base (x_b, z_b) were manually digitized for each profile as the points of maximum curvature.

The main parameter of interest for quantifying dune erosion is the volume eroded per unit beach width per unit time. This was estimated as

$$\Delta V = \sum_{z_b}^{z_c} \Delta x \ \Delta z \tag{8}$$

where ΔV was estimated over consecutive 15 minute time segments (Fig. 9).

Maximum dune erosion rate occurred at hour 10, when wave height, period, and water level were increased. Erosion from the dune decreased as waves maintained a constant height between hours 10–12, and flux from the dune increased again after hour 12, when wave height, period and water level were increased to the maximum for the experiment. The maximum flux after hour 12 was less than that immediately after hour 10, despite the larger waves and higher surge level. The large magnitude flux at hour 17.25 is likely due to error in position of the dune during a time when image contrast was low. Video observations indicate that slumping did not occur during this period.

5.2. Wave runup

The first parameterization for estimating dune erosion volume is $(R - z_b)$. While Sallenger (2000) recommended the 2% exceedance as the relevant runup statistic for dune erosion, the appropriateness of this statistic has never been tested. We have investigated the performance of 2%, 7%, 16%, 23%, and 30% exceedance values. Observed exceedance values were calculated from the cumulative probability distribution of R, the elevation of individual maxima above the still water line identified from the time series of runup elevations (Stockdon et al., 2006). Assuming a Gaussian distribution of swash statistics (Stockdon et al., 2006), the exceedance values tested correspond to the combined mean water level plus $n_\sigma = 2$, 1.5, 1.0, 0.75, and 0.5 times the standard deviations of the swash time series (σ_s).

Observed exceedance elevations were compared with Eq. (1), modified to account for the different exceedance elevations by including n_σ, the coefficient to adjust the number of σ_s considered

$$R_n = 1.1\left(0.35\beta(H_oL_o)^{1/2} + \frac{\left[H_oL_o\left(0.563\beta^2 + 0.0004\right)\right]^{1/2}}{2}\frac{n_\sigma}{2}\right). \tag{9}$$

β in Eq. (9) was parameterized in four ways: 1) with the time-varying mean beach slope between the still water line and the base of the dune, β_s, 2) with the observed beach slope at hour 8, prior to the onset of dune erosion, β_0, and 3, 4) with the time varying mean beach slopes appropriate to in the active swash regions, $\langle\eta\rangle \pm n_\sigma\sigma_s$, denoted $\beta_{1\sigma}$ and $\beta_{2\sigma}$ for R_{16} and R_2, respectively. Only results for R_2 and R_{16} will be presented in detail, because later it will be shown that R_{16} was most proficient at predicting volume of sediment eroded from the dune. In addition, beach slopes can be computed by least squares or as end-point mean values. Each method weights the foreshore profile data differently.

First, we present results for observations of R_2 which was lowest between hours 8 and 10 (Table 1), corresponding to minimum storm wave conditions and water level. R_2 increased at hour 10 when wave conditions and water level increased then remained relatively constant (standard deviation of R_2 was 0.03 m) through hour 20, although wave conditions and water level increased at hour 12 and decreased at hour 18. Based on observations of the horizontal excursion of runup past the dune crest, it is apparent that overtopping occurred between hours 10 and 20. The probability density function of R between hours 12 and 14 was truncated once runup reached the dune top (Fig. 10). This truncation precludes testing runup models for 2% exceedance. Therefore, we will focus on observations and parameterizations of R_{16} for the rest of this section.

Like R_2, R_{16} was lowest between hours 8 and 10 (Fig. 11). In contrast to R_2, R_{16} was never truncated by reaching the dune crest, so

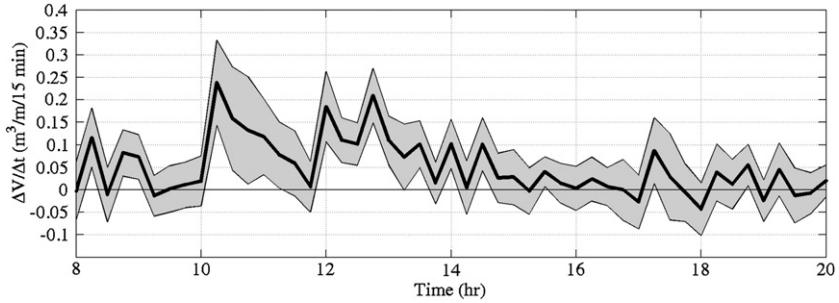

Fig. 9. The volume of sediment eroded from the dune calculated with Eq. (8) is plotted in black. The gray region defines the 95% confidence interval on volume change based on error bars for the stereo method from Eq. (6).

Table 1
Wave conditions and measured runup during dune erosion.

Time (h)	H_s (m)	T_p (s)	$\overline{R_2}$ (m)	σR_2 (m)
8–10	0.62	3.01	0.56	0.03
10–12	1.01	3.85	1.03	0.01
12–18	1.13	4.68	0.97	0.03
18–20	1.04	4.83	1.01	0.02

responded to changing wave conditions and water levels at hours 10, 12, and 18. Although incoming wave height and period were constant between hours 12 and 18, observed runup dropped significantly after hour 14.5 (Fig. 11, thick black line). Possible reasons for this anomalous drop are included in the later discussion section. Runup results are presented in two-hour blocks to allow isolation of these unknown effects. All other results are based on the entire dataset.

Next, we compare observations of R_{16} with predictions from Eq. (9) but using different definitions of beach slope. Results are plotted in Fig. 14 and summarized in Tables 2 and 4 (bias) and 3 and 5 (RMSE). The experiment included periods for which runup minimally exceeded the dune base (hours 8–10 and 18–20; the Sallenger (2000), swash regime) and times of significant swash impact with the vertical dune face (hours 10–18; the Sallenger collision regime). Since Eq. (9) was based on swash regime processes on simple foreshores, it should provide reasonable predictions for the swash regime periods but may be systematically in error during times of collision regime. Examining data from swash regime conditions, it is apparent that $\beta_{1\sigma}$ provides the best predictions (Tables 2 and 3, second column), followed by β_0 (Tables 2 and 3, fourth column). While the Stockdon et al. (2006) study used $\beta_{2\sigma}$ to model their statistic of R_2, $\beta_{1\sigma}$ should be more appropriate for the $1\sigma_s$ statistic, R_{16}. In fact, $\beta_{2\sigma}$ under-predicts R_{16} throughout the experiment.

During collision regime conditions, hours 10–14, all estimates under-predict the observed runup. Since Eq. (9) is based on simple foreshore profiles seaward of dunes, this under-estimate is not a surprise but could be empirically adjusted to correct for dune impact by multiplication by dune factor, K_d. Mean values of K_d for hours 10–14 are listed in Table 6. Again, $\beta_{2\sigma}$ strongly underestimates observed R_{16} and is not considered an attractive option from either a theoretical or observational point of view. β_s provides estimates that are reasonable but noisy, especially when used in the end-point mode. The best choices seem to be $\beta_{1\sigma}$ and β_0 as these provide stable estimates that can be easily corrected for dune runup by multiplication by K_d. RMSE and bias from the least squares and endpoint methods for $\beta_{1\sigma}$ and β_0 were within 0.01 m of each other.

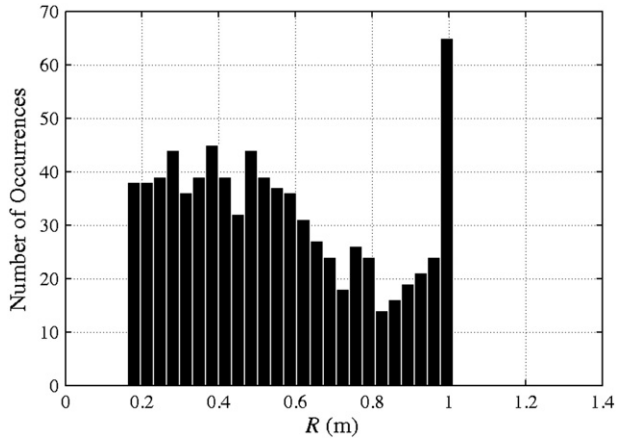

Fig. 10. The histogram of runup maxima is plotted between hours 12 and 14. The histogram is truncated at the elevation of the dune crest because waves were overtopping the dune.

5.3. Position of the dune base

The second component of the first parameter for estimating fluid forcing of dune erosion (LEH04; Eq. (4)) is the elevation of the dune base, z_b. If the dune base elevation rises as the dune erodes, the erosion rate will be reduced. This could be an important feedback in the system. Thus, successful prediction of dune erosion requires knowledge of the expected trajectory of the eroding dune toe.

If we describe the dune toe trajectory as following a slope, β_T, two end member retreat trajectories exist. The first would be direct landward erosion so that z_b never changed

$$\begin{aligned} z_b(t) &= z_b(0) \\ \beta_T &= 0. \end{aligned} \tag{10}$$

The second end member is that erosion moves the dune toe directly up the foreshore slope

$$\begin{aligned} z_b(t) &= \beta_T(t)x(t) + z_b(0) \\ \beta_T &= \beta_f(0). \end{aligned} \tag{11}$$

More generally, we can express the observed trajectory as a fraction of the foreshore beach slope. Previous laboratory observations suggest that a retreat along the foreshore beach slope ($\beta_T/\beta_f(0) = 1$) is reasonable (LEH04).

The measured trajectory of z_b is shown in Fig. 12. On average the dune toe trajectory follows a slope of 0.09 ($R^2 = 0.87$, significant at the 95% confidence interval), but with some variations associated with slump events. Compared to the foreshore slope, $\beta_f(0)$, of 0.17, the ratio, $\beta_T/\beta_f(0)$, averaged over the experiment was 0.54, inconsistent with the LEH04 results. The effect of assuming this trajectory on estimation of eroded volume will be tested in Section 5.5.

5.4. Period of exposure to runup

The final parameterization in estimating dune erosion using LEH04 is the non-dimensional period that dunes were exposed to runup. Period of exposure was parameterized in Eq. (3) as t/T which is a proxy for the number of collisions with the dune. We also tested an alternative parameterization, where number of collisions was quantified by incorporating information about the probability distribution of wave runup, $p(z_R)$, and z_b. In this parameterization, the number of collisions, N_c are defined as

$$N_c = [P(z_R + z_{SWL} > z_b)] \cdot \frac{t}{T_p} \tag{12}$$

where $P(z_R)$ is assumed to be a Gaussian distribution defined by $\langle\eta\rangle$ and σ_s derived from Eq. (1). z_R is the runup elevation composed of setup and swash, and z_{SWL} is the elevation of the still water level. z_b was estimated assuming a retreat of the dune base along β_T and a known cross-shore dune position.

Observations of the number of collisions are shown in Fig. 13 (heavy line) and were determined by counting the times the digitized runup edge exceeded the dune base.

N_c was highest between hour 8–8.25 when wave period was the shortest of any time during the storm (3.1 s) and the z_b was the lowest. N_c decreased rapidly as z_b increased during the first 2 h of storms waves. The number of collisions increased at hours 10 and 12, when wave conditions and water levels increased, then decreased as z_b increased between hours 12 and 20. Finally, N_c dropped to only 2–3 collisions after hour 20, when waves and water level were decreased.

The parameterization for number of collisions as t/T overestimated the observed value (bias = 155 collisions, RMSE = 160 collisions, $R^2 = 0.53$). The over estimation was largest at the end

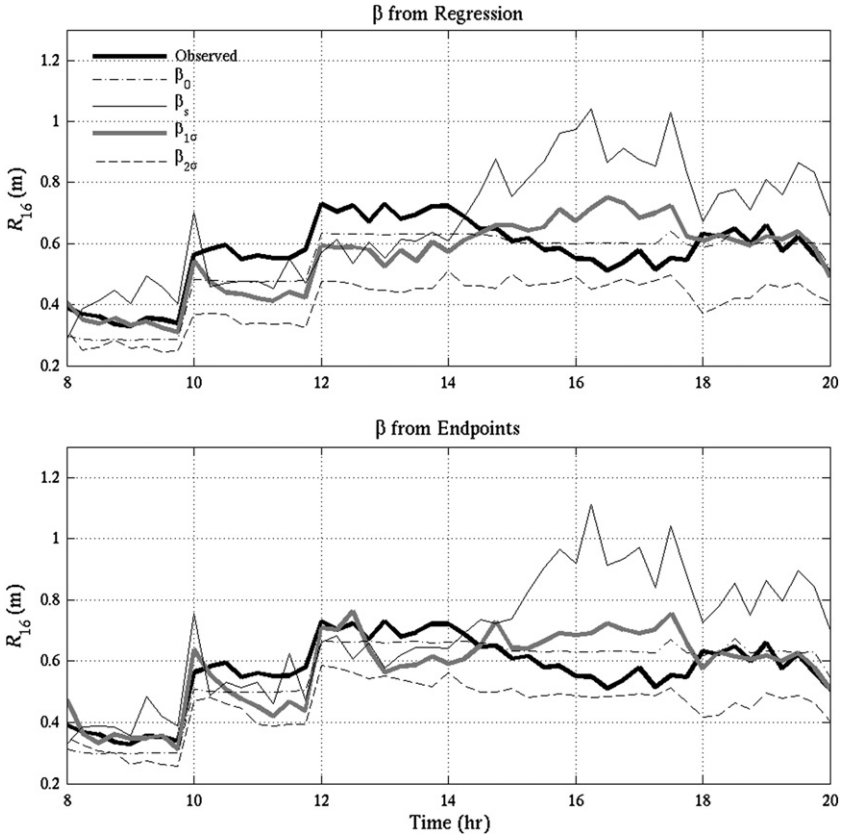

Fig. 11. Observed and calculated R_{16} are plotted for the four different definitions of beach slope. Each definition of beach slope was calculated using regression (upper plot) and end point methods (lower plot). β_0 and $\beta_{1\sigma}$ calculated by regression produced results most similar to the observations. The comparisons are quantified in Tables 2–5.

of the experiment, when few waves reached the dune. Results improved using Eq. (12) and assuming retreat of the dune along β_T and z_R parameterized by $\langle\eta\rangle$ and σ_s from Eq. (1) with $\beta_s(t)$ (bias = −27 collisions, RMSE = 34 collisions, $R^2 = 0.75$). After hour 12, z_b was overestimated and N_c was consequently underestimated.

5.5. Comparison with observed erosion

The observations of $(R_n - z_b)$ and N_c were compared with observed dune response to determine contribution of each variable to eroded volume (Fig. 14). The assumption that $(R_n - z_b)$ was linearly related to dune erosion volume was tested first. The correlation-squared for all runup exceedance levels, n, was between 0.30 and 0.60, all significant at the 95% level. However, the correlation-squared for R_{16} was highest. Next, the observations of N_c were compared to dune response. The correlation-squared was 0.37, significant at the 95% level.

Eq. (3) was compared with observations of dune erosion in two ways: using observed forcing and known beach profiles to demonstrate the model reliability given known conditions, and using the initial beach profile and parameterized forcing based on offshore conditions, to demonstrate how the model would perform in a forecast or hindcast scenario where runup and beach profile throughout the storm were not measured.

Given known forcing from R_{16}, beach profiles, and $C_s = 1.34 \times 10^{-3}$ (following LEH04) Eq. (3) reproduced 64% of the observed variance in dune erosion rate (Fig. 15, upper plot). Bias in eroded volume for LEH04 was 0.03 m^3/m/15 min and RMSE was 0.05 m^3/m/15 min. Initially, eroded volume was over-predicted but eroded volume rapidly tapered as the dune base eroded upward and was less exposed to runup. Between hours 10 and 12 the model overestimated eroded volume, but the trend toward decreasing erosion with time matched observations. Between hours 12 and 20, the model tracked observed eroded volume

Table 2
Parameterization bias in m during dune erosion using regression slope.

Time (h)	$\overline{\Delta R_{16}}$ Eq. (9) $\beta_s(t)$	$\overline{\Delta R_{16}}$ Eq. (9) $\beta_{1\sigma}(t)$	$\overline{\Delta R_{16}}$ Eq. (9) $\beta_{2\sigma}(t)$	$\overline{\Delta R_{16}}$ Eq. (9) $\beta_s(0) = 0.17$
8–10	0.06	0.01	−0.09	0.07
10–12	−0.06	−0.11	−0.22	−0.09
12–14	0.11	−0.13	−0.25	−0.08
14–16	0.16	0.01	−0.16	−0.02
16–18	0.38	0.16	−0.07	0.06
18–20	0.16	0.00	−0.19	−0.01
8–20	0.1	−0.01	−0.16	−0.03

Table 3
Parameterization RMSE in m during dune erosion using regression slope.

Time (h)	RMSE ΔR_{16} Eq. (9) $\beta_s(t)$	RMSE ΔR_{16} Eq. (9) $\beta_{1\sigma}(t)$	RMSE ΔR_{16} Eq. (9) $\beta_{2\sigma}(t)$	RMSE ΔR_{16} Eq. (9) $\beta_s(0) = 0.17$
8–10	0.09	0.02	0.09	0.07
10–12	0.10	0.12	0.22	0.09
12–14	0.12	0.14	0.25	0.08
14–16	0.21	0.08	0.17	0.04
16–18	0.39	0.17	0.08	0.07
18–20	0.17	0.03	0.19	0.03
8–20	0.21	0.10	0.17	0.06

Table 4
Parameterization bias in m during dune erosion using end point slope.

Time (h)	$\overline{\Delta R_{16}}$ Eq. (9) $\beta_s(t)$	$\overline{\Delta R_{16}}$ Eq. (9) $\beta_{1\sigma}(t)$	$\overline{\Delta R_{16}}$ Eq. (9) $\beta_{2\sigma}(t)$	$\overline{\Delta R_{16}}$ Eq. (9) $\beta_s(0)=0.17$
8–10	0.04	0.01	−0.06	0.02
10–12	−0.02	−0.01	−0.14	−0.05
12–14	−0.07	−0.06	−0.16	−0.06
14–16	0.14	0.02	−0.13	−0.04
16–18	0.41	0.16	−0.05	0.01
18–20	0.20	−0.01	−0.16	0.09
8–20	0.12	0.01	−0.11	0.00

Table 5
Parameterization RMSE in m during dune erosion using end point slope.

Time (h)	RMSE ΔR_{16} Eq. (9) $\beta_s(t)$	RMSE ΔR_{16} Eq. (9) $\beta_{1\sigma}(t)$	RMSE ΔR_{16} Eq. (9) $\beta_{2\sigma}(t)$	RMSE ΔR_{16} Eq. (9) $\beta_s(0)=0.17$
8–10	0.06	0.03	0.06	0.05
10–12	0.10	0.10	0.14	0.06
12–14	0.08	0.09	0.16	0.05
14–16	0.20	0.08	0.13	0.04
16–18	0.41	0.16	0.06	0.10
18–20	0.25	0.03	0.16	0.04
8–20	0.21	0.09	0.12	0.06

Table 6
Empirical runup correction factor (K_d).

Time (h)	K_d Eq. (9) $\beta_{1\sigma}(t)$	K_d Eq. (9) $\beta_s=0.17$
10–12	1.26	1.12
12–14	1.23	1.19

well. The observed eroded volume was noisier than the model; some of the observed noise is due to errors in the stereo technique.

Given parameterized forcing from offshore wave conditions, initial beach slope and Eq. (9) with $n=16$, Eq. (11) with $\beta_T=0.54$, and Eq. (12), the eroded volume was calculated, then the profile was updated assuming retreat along β_T, and eroded volume calculated for the next 15 minute interval. The modeled explained 49% of observed variance in erosion rate (Fig. 18, lower plot). Bias was 0.00 m^3/m/15 min, and was 0.05 m^3/m/15 min. In terms of dune morphology, the model underestimated retreat of the dune base by 0.36 m out of 5.04 m of erosion over the full 12 h of active erosion.

6. Discussion

6.1. Stereo video analysis

Stereo video appears to provide a useful tool for the non-intrusive measurement of an eroding foreshore and dune system. An objective confidence estimate reported in real world coordinates yet based totally on video observations was developed to quantify data of uncertain quality. However, two areas of improvement could be made. First, lighting for the experiment was sub-optimal in two ways. At times, strong morning sunlight saturated image intensities, particularly on the dune crest. With limited contrast, estimates were noisy although the confidence intervals were correspondingly large. Similarly, under some lighting conditions, there was little optical contrast on the eroding dune front. This was a particular problem in the vicinity of the strong contrast signal at the dune crest, and correlation windows were often dominated by the dune crest optical signal over a broad range of lags.

Similarly, performance of the stereo algorithm depends on the resolution of the images. As shown in Fig. 5, the application of a correlation window over the discrete feature of the dune crest resulted in an overhang. RMSE due to this issue was initially 0.04 m, but increased to 0.08 m (Figs. 5 and 7). Low image variance at the scarp combined with lower resolution precluded using a smaller correlation window to improve the overhang in this experiment. Issues of resolution should be considered when designing a stereo installation.

While the described stereo methods could provide a useful solution to field sampling of an eroding dune during a storm, it must be recognized that field installations will have some challenges. The principal issue would be the placement of cameras to provide views of a seaward facing dune front. This will only be possible if seaward mount points are available, for example a pier or piling. de Vries et al. (2011) recently estimated wave height with a pier mounted stereo rig aimed toward the shoreline. Alternatively, cameras could be mounted from a tower or high rise building and vertically separated. (Clarke and Holman, 2006) successfully imaged 3-dimensional views of the foreshore and unscarped dune from the 43 m tower at the Army Corps Field Research Facility at Duck, NC, USA. Although the dune scarp would be obscured during a storm, it would be possible to track the position of the dune crest as it eroded.

A second complication in field applications is lighting and weather. Image contrast will vary with sun angle, and the optimal position of the sun relative to the camera depends on a variety of factors including time of year, camera view direction, and beach morphology. Sun angles that avoid over exposure of the image are required, so images collected in early morning on a sunny day on an east facing coast, and late in the day on a west facing coast are likely to provide little useful information. Sun angles that produce dark shadows where image contrast is very low result in low correlations in the feature matching technique. Sun angles that minimize reflection of light off water draining from the foreshore are ideal. Overcast skies frequently produce the best quality images because the clouds diffuse the sunlight, eliminating reflections that can be problematic for the stereo technique. To avoid image distortion by raindrops during a storm, camera housings may equipped with a spinning window.

6.2. Runup and dune erosion

This experiment is one of the first where wave runup was quantitatively observed during collision and overtopping conditions. The Sallenger (2000) model defines these erosion regimes in terms of the 2% exceedance level of runup, R_2, while LEH04 defines a level that is functionally equivalent to R_2. However, there has been little investigation into the sensitivity of erosion predictability to the selected exceedance level.

In our observations, collision and overtopping regimes as well as erosion rates are better predicted by a higher exceedance level, R_{16}. The regression coefficient comparing runup statistics to eroded volume is the maximum for R_{16}. While the maximum is not strong, there is no evidence that R_2 is better. Similarly, while R_2 at times exceeded z_c, indicating the overtopping regime, there was no evidence for significant onshore sediment transport, as implied by Sallenger (2000) and Stockdon et al. (2007). Therefore, we suggest that although all the runup exceedance values tested were significantly related to magnitude of dune erosion, the relevant statistic for dune erosion risk assessment should be lower than R_2. We recommend the use of R_{16} for predictive purposes.

Runup is known to depend on foreshore beach slope, but since natural beach profiles are typically concave, a number of interpretations of slope are possible. We examined predictability of runup

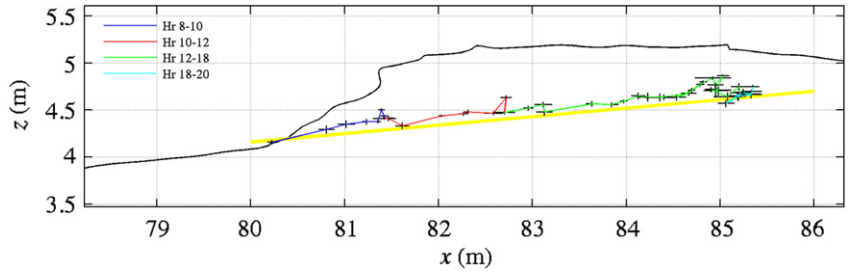

Fig. 12. The initial beach profile and trajectory of the dune base over the experiment are plotted with error bars on the position of the dune base. The yellow line, with slope β_T is the retreat trajectory.

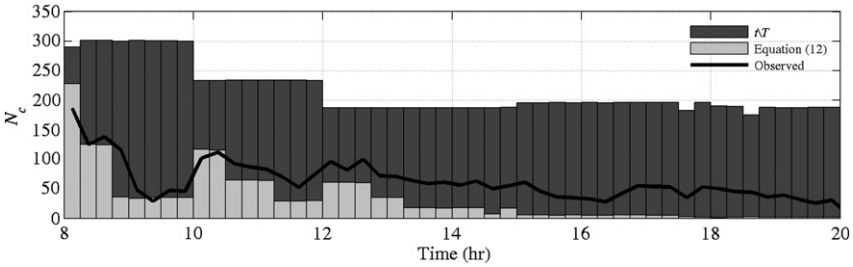

Fig. 13. The observed N_c compared with N_c modeled using Eq. (12) and N_c estimated using LEH04 parameterization of t/T. Eq. (12) improves the parameterization of N_c over the original parameterization in LEH04.

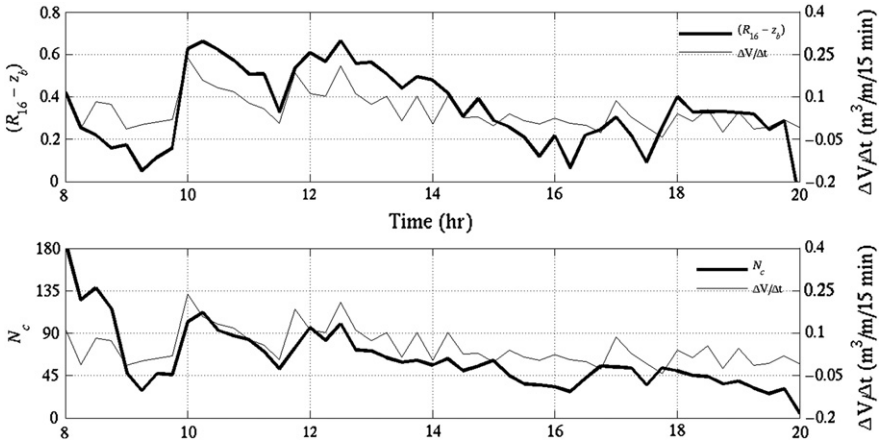

Fig. 14. The observed forcing, $(R_{16}-z_b)$ (upper plot) and N_c (lower plot), are compared with the observed dune erosion volume. The squared-correlations were 0.60 and 0.37, respectively; both are significant at the 95% confidence interval and demonstrate that while both components of the wave impact model have some skill at estimating dune erosion rate, $(R_{16}-z_b)$ is more important.

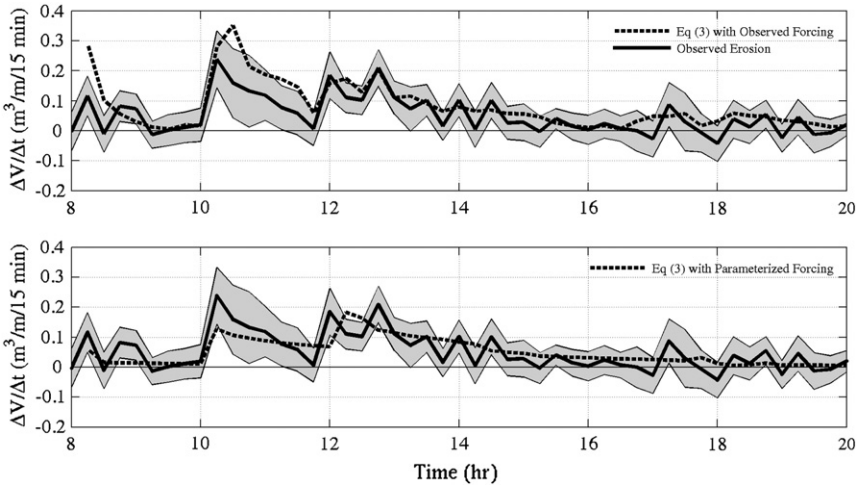

Fig. 15. Results of LEH04 with known forcing and beach profiles (upper plot) and LEH04 with parameterized forcing (lower plot) compared with observed dune erosion fall within the error bars of the measurement technique.

(Eq. (9)) based on four different definitions of beach slope. In addition, slopes can be defined either by least squares or by end-point calculation. For hours 8–10 and 18–20 when runup was mostly confined to the foreshore, comparison between runup observations and Eq. (9) allow testing of the various choices of slope. But for times of active dune erosion, the fit between observed runup and Eq. (9) is not as good (Tables 2–5) since this equation does not purport to represent runup statistics on such a complicated profile.

Based on the comparisons of parameterized R_{16} and observations in Tables 2–5, the foreshore beach slope $\beta_{1\sigma}$, defined between $\langle\eta\rangle \pm \sigma_s$, produced better results (RMSE = 0.10 m) than mean slope defined between the still water line and the dune base, β_s (RMSE = 0.21 m). However, the predictions of R_{16} associated with β_0 (RMSE = 0.06 m), the time-independent slope from still water level to the dune base at the beginning of the storm, are slightly better than predictions based on $\beta_{1\sigma}$, and are considerably easier to estimate. Thus, the comparison supports the hypothesis of Stockdon et al. (2007), that the initial mean beach slope is a useful parameterization of slope when time dependent slope is unknown. The success of the parameterization with the initial beach slope also suggests that feedback between beach slope and runup may be of secondary importance.

Both least squares and end point methods for estimating beach slope from Eq. (9) were tested. Runup results were similar for both methods, with a RMSE of 0.09 m over the experiment for the end-point method and a RMSE of 0.10 m for the least squares method. Least squares methods typically yielded shallower slopes by reducing the relative weight of the steeper dune face compared to the flatter foreshore slope.

Runup data from hours 14.5 to 18 appear anomalous (Fig. 11). Despite uniform wave conditions from hours 12 to 18 at the wave paddle (Fig. 3), after hour 14.5 the foreshore beach slope rapidly steepened and runup levels dropped. Since Eq. (9) predicts a positive relationship between these two variables, predictive models are unable to mimic this behavior, so error statistics are larger. It is not totally clear why this happened, although it appears to be related to changes in the surf zone beach profile. For the time period in question, a sand bar grew and moved offshore. Incident waves broke over the bar during the largest wave conditions between hours 12–18, likely reducing incident swash magnitudes. Similarly, measured infragravity energy in the tank was also reduced, perhaps related to changes in the breakpoint-generated infragravity motions at the particular bar position (Symonds and Bowen, 1984). The physics of these observed changes deserves further investigation.

The parameterization of the dune base trajectory with Eq. (11) appears to be the weakest parameterization in the model. At hour 14, there is an increase in slope of the retreat trajectory (Fig. 12), possibly related to the decrease in infragravity energy observed in runup. A strong connection appears to exist between trajectory of the dune base and eroded volume from the dune. We observed that the dune eroded to the point where the elevation of the base minimized contact between the runup and the dune face and that the dune base and foreshore beach slope adjusted over the course of the experiment. This may indicate a change from slumping dominated transport at the dune face to energetics dominated transport of sediment off the foreshore. A model combining the processes of dune slumping through slope instability and swash zone sediment transport is needed to model the gradients in sediment transport resulting in exposing or limiting the dune scarp to runup. Further work is needed to parameterize the dune base trajectory in simple models, and including dune slumping as a separate process may be necessary to model trajectory in a full cross-shore sediment transport model.

Given known forcing at the dune, Eq. (3) reproduced 64% of the observed variance in the erosion rate. This suggests that many of physics of dune erosion are encapsulated by the forcing and C_s in Eq. (3). We also implemented Eq. (3) using offshore forcing and initial beach slope in a way that would be representative of a forecasting or hindcasting exercise. In this case, the model explained 49% of the observed variance in erosion rate, a 15% drop over known forcing, and bias and was nearly the same as for the known forcing. The final position of the modeled dune was within 0.36 m of the observed retreat distance of 5.06 m. The retreat distance scaled to the prototype was 30.4 m, similar in magnitude to the maximum retreat of dunes during the Assateague Island storm (Fauver, 2005). The model may be useful for predicting dune erosion at prototype scales.

In contrast to many dune erosion models which invoke an avalanching criteria, we hypothesize that dune slumping should be modeled using an understanding of slope stability. For example, runup was in contact with the dune for approximately 45% of the time between hours 8 and 8.25, yet no slumping and little erosion of the dune was observed. At that time, the dune was relatively low sloping ($\tan\beta = 0.5$), and although this exceeds the avalanching criteria for some models, no slumping occurred, suggesting that the slope was relatively stable. Later in the experiment, a steep scarp developed in the region where waves were active. Using the avalanching criteria, a steep scarp on a wet slope should not exist. In contrast, knowledge of slope stability suggests that the increase in shear strength due to capillary forces in the wet dune should produce the scarp that was observed. Further work must be conducted to study the effect of infiltration of water into the dune, and the balance of forces on the scarp.

7. Conclusions

We have developed a remote sensing technique for making three dimensional observations of the subaerial beach and dune under conditions of storm dune erosion. Observations were made at higher temporal and spatial resolutions (every 15 min for the full profile; 0.04 and 0.10 m resolution in the vertical and horizontal, respectively, over the entire dune and foreshore surface) than is possible with in situ surveying methods. Bias of the stereo technique ranged between −0.03 m and 0.02 m, depending on location of the dune and foreshore in the image. Root mean square difference between stereo observations and surveyed observations ranged between 0.03 m and 0.08 m, depending on image variance and smoothing of the dune crest by the correlation window. Errors were on the order of one to two pixels. A method to estimate confidence intervals based solely on image information was developed and found to be effectively parameterize scatter about the mean surface in 98% of the observations.

We quantified the time-dependent wave runup and dune erosion during a wave tank dune erosion experiment modeled after an actual storm hydrograph. Based on observations, we found that R_{16} was the appropriate runup statistic for quantifying dune erosion, a less extreme statistic than the normally-accepted 2% exceedance value, R_2. We tested the dependency of R_{16} on beach slope with a number of beach slope estimators and found the two best estimators were $\beta_{1\sigma}$, the time-dependent slope for the region within one standard deviation of the mean swash, and β_0, the time-independent slope between the still water line and the dune toe at the beginning of erosion. The success of β_0 supports the hypothesis of Stockdon et al. (2007) that β_0 is a reasonable estimate of foreshore beach profile during a storm.

The dune base eroded at a relatively constant trajectory along β_T, which was 0.54 β_0, roughly half way between a simple up-slope and a totally horizontal trajectory. This simple relationship has predictive skill for estimating retreat trajectory in the absence of detailed model for cross-shore sediment transport ($R^2 = 0.87$).

LEH04 includes a parameterization, t/T that is a proxy for number of runup collisions with the dune. An improved parameterization was developed, incorporating a Gaussian distribution for runup and elevation of the dune base. Most of the error in N_c can be attributed to error in elevation of the dune base

A simple model of dune erosion (LEH04) that combines estimates of dune face exposure to runup with a proxy for the number of swash

impacts successfully reproduced 64% of the observed variance in erosion rate with known forcing at the dune and 49% of the observed variance in erosion rate using parameterized offshore forcing. Over the course of the modeled storm, the modeled dune base retreated 4.68 m or 93% of the observed retreat distance. This suggests that practical prediction of dune erosion using parameterized storm inputs will be useful.

Acknowledgments

The authors would like to thank Linden Clarke for early development of the stereo code, John Stanley for his hard work on this and other Argus projects, and Peter Ruggiero and Tim Maddux for data collection and project development. This work was completed with funding from the Oregon Sea Grant, the United States Geological Survey, and the Office of Naval Research.

References

Allan, J.C., Komar, P.D., 2006. Climate controls on us west coast erosion processes. Journal of Coastal Research 22 (3), 511–529.
Changnon, S.A., 2000. El Niño 1997–1998: The Climate Event of the Century. Oxford University Press, New York. 215 pp.
Clarke, L., Holman, R., 2006. High resolution measurements of beach face morphology using stereo video cameras. Eos Transactions AGU 87 (52) Fall Meet. Suppl., Abstract OS23D-07.
de Vries, S., Hill, D.F., de Schipper, M.A., Stive, M.J.F., 2011. Remote sensing of surf zone waves using stereo imaging. Coastal Engineering 58 (3), 239–250.
Dean, R.G., Dalrymple, R.A., 2002. Coastal Processes with Engineering Applications. Cambridge University Press, Cambridge, UK.
Dette, H.H., et al., 2002. Application of prototype flume tests for beach nourishment assessment. Coastal Engineering 47 (2), 137–177.
Egnal, G., Mintz, M., Wildes, R.P., 2004. A stereo confidence metric using single view imagery with comparison to five alternative approaches. Image and Vision Computing 22 (12), 943–957.
Fauver, L.A., 2005. Toward Predicting Barrier Island Vulnerability Simple Models for Dune Erosion. University of South Florida, Tampa, Fla.
Fisher, J.S., Overton, M.F., Chisholm, T., 1986. Field measurements of dune erosion. 20th International Conference on Coastal Engineering, Taipei, Taiwan, pp. 1107–1115.
Graham, N.E., Diaz, H.F., 2001. Evidence for intensification of north pacific winter cyclones since 1948. Bulletin of the American Meteorological Society 82 (9), 1869–1893.
Hartley, R.I., Zisserman, A., 2004. Multiple View Geometry in Computer Vision. Cambridge University Press, Cambridge.
Holland, K.T., Holman, R., 1997. Video estimation of foreshore topography using trinocular stereo. Journal of Coastal Research 13 (1), 81–87.
Holman, R.A., Stanley, J., 2007. The history and technical capabilities of Argus. Coastal Engineering 54 (6–7), 477–491.
IPCC, 2007. Climate change 2007: the physical science basis. Contribution of Working Group I to the Fourth Assessment Report of the Intergovernmental Panel on Climate Change. Cambridge University Press, Cambridge, United Kingdom.
Larson, M., Erikson, L., Hanson, H., 2004. An analytical model to predict dune erosion due to wave impact. Coastal Engineering 51 (8–9), 675–696.
Overton, M.F., Fisher, J.S., 1988. Simulation modeling of dune erosion. International Conference on Coastal Engineering, Costa del Sol-Malaga, Spain, pp. 1857–1867.
Overton, M.F., Fisher, J.S., Hwang, K.N., 1994. Development of a dune erosion model using supertank data. Proceedings of the Twenty-Fourth International Conference on Coastal Engineering, Kobe Japan, pp. 2488–2502.
Plant, N.G., Holland, K.T., Puleo, J.A., 2002. Analysis of the scale of errors in nearshore bathymetric data. Marine Geology 191 (1–2), 71–86.
Pye, K., Blott, S.J., 2008. Decadal-scale variation in dune erosion and accretion rates: an investigation of the significance of changing storm tide frequency and magnitude on the Sefton Coast, UK. Geomorphology 102 (3–4), 652–666.
Ruggiero, P., Komar, P.D., McDougal, W.G., Marra, J.J., Beach, R.A., 2001. Wave runup, extreme water levels and the erosion of properties backing beaches. Journal of Coastal Research 17 (2), 407–419.
Sallenger Jr., A.H., 2000. Impact scale for barrier islands. Journal of Coastal Research 16 (3), 890–895.
Stockdon, H.F., Holman, R.A., Howd, P.A., Sallenger, A.H., 2006. Empirical parameterization of setup, swash, and runup. Coastal Engineering 53 (7), 573–588.
Stockdon, H.F., Sallenger, J.A.H., Holman, R.A., Howd, P.A., 2007. A simple model for the spatially-variable coastal response to hurricanes. Marine Geology 238 (1–4), 1–20.
Sun, C., 2002a. Fast optical flow using 3D shortest path techniques. Image and Vision Computing 20 (13–14), 981–991.
Sun, C., 2002b. Fast stereo matching using rectangular subregioning and 3D maximum-surface techniques. International Journal of Computer Vision 47 (1), 99–117.
Symonds, G., Bowen, A., 1984. Interactions of nearshore bars with incoming wave groups. Journal of Geophysical Research 89 (c2), 1953–1959.
van Gent, M.R.A., van Thiel de Vries, J.S.M., Coeveld, E.M., de Vroeg, J.H., van de Graaff, J., 2008. Large-scale dune erosion tests to study the influence of wave periods. Coastal Engineering 55 (12), 1041–1051.
van Thiel de Vries, J.S.M., van Gent, M.R.A., Walstra, D.J.R., Reniers, A.J.H.M., 2008. Analysis of dune erosion processes in large-scale flume experiments. Coastal Engineering 55 (12), 1028–1040.